https://doi.org/10.17221/79/2023-RAE

Digital image processing for preliminary detection of infected porang (*Amorphophallus muelleri*) seedlings

Aryanis Mutia Zahra[1], Noveria Anggi Nurrahmah[1], Sri Rahayoe[1], Rudiati Evi Masithoh[1], Muhammad Fahri Reza Pahlawan[2], Laila Rahmawati[3]*

[1]*Department of Agricultural and Biosystems Engineering, Faculty of Agricultural Technology, Universitas Gadjah Mada, Yogyakarta, Indonesia*
[2]*Department of Smart Agriculture Systems, College of Agricultural and Life Science, Chungnam National University, Daejeon, South Korea*
[3]*Research Center for Food Technology and Processing, National Research and Innovation Agency, Yogyakarta, Indonesia*

**Corresponding author: aryanismutiazahra@ugm.ac.id*

Citation: Zahra A.M., Nurrahmah N.A., Rahayoe S., Masithoh R.E., Pahlawan M.F.R., Rahmawati L. (2024): Digital image processing for preliminary detection of infected porang (*Amorphophallus muelleri*) seedling. Res. Agr. Eng., 70: 111–121.

Abstract: Porang (*Amorphophallus muelleri*) is an Indonesian parental plant tuber developed vegetatively from bulbils during dormancy and harvested through petiole detachment for the industrial production of glucomannan. Pathogenic fungi and whiteflies can cause infection during harvesting and storage, destructing plant cells as well as reducing seed quality and crop yields. Therefore, this study aimed to develop a calibration model for detecting infected and non-infected porang bulbils using a computer vision system. Image parameters such as colour (red, green, blue – RGB and hue, saturation, intensity – HSI), texture (contrast, homogeneity, correlation, energy, and entropy), and dimensions (width, area, and height) were evaluated on 90 samples in three positions. The results showed that the majority of image quality properties were significantly associated with non–infected and infected porang bulbils as showed by Pearson correlation values of 0.901 and 0.943, respectively. Discriminant analysis based on image attributes effectively classified non-infected and infected seedlings, achieving a model accuracy of 97.0% for correctly classified cross-validated grouped cases. Therefore, computer vision can be used for the preliminary detection of fungal infection in porang bulbils, as evidenced by its high accuracy and outstanding model performance.

Keywords: discriminant analysis; gray–level cooccurrence matrix; model performance; seed quality; vegetative phase

Amorphophallus muelleri Blume, known locally as porang, is an Indonesian parental plant tuber in the Araceae family (Anggela et al. 2021; Nurlela et al. 2022). This plant contains the highest concentration of glucomannan compared to other sources, reaching 90.98% in the tuber (Yanuriati et al. 2017), and 94.45% in the flour (Anggela et al. 2021). Glucomannan is a hemicellulose-type polysaccharide that has chain links of glucose, galactose, and mannose with β-1,4-linked *D*-mannose and *D*-glucose monomers. Despite the high water solubility, viscosity, gelation, and hydrocolloid fibre content, porang tubers are unpleasant due to their high calcium oxalate composition (Sakaroni et al. 2019; Nurlela et al. 2022; Sarifudin et al. 2022). Porang is widely used in the food, pharmaceutical, biological, and cosmetic industries. However, the tubers are often sliced and dried without additional glucomannan extraction as a highly demanded export commodity (Yanuriati et al. 2017; Sakaroni et al. 2019; Nurlela et al. 2022).

https://doi.org/10.17221/79/2023-RAE

In January–February 2021, porang exports increased by 32.31% to USD 1.52 million and 965.5 tons, compared to the same quarter in the previous year, with China, Thailand, and Malaysia being the top three export destinations. Although the export market has expanded, only 20% of dry chip demand was satisfied (Riptanti et al. 2022). This is mainly due to the limited cultivation in Indonesia. There are significant opportunities to increase the export market share through intensive management of cultivation, including preparing land for nurseries and planting, maintaining plants and land, harvesting tubers, and developing porang cultivation as an agro-forestry and export product (Dermoredjo et al. 2021; Riptanti et al. 2022). One method for intensive production is the use of leaf tubers or bulbils, found on the branches of leaf stalks (Nugrahaeni et al. 2021).

The three primary sources of porang seedlings include tubers (called corms), bulbils (small bulbs developed in leaf axils), and seeds. Regarding cost and environmental impact, bulbils are recognised as the best option among the three alternatives. The production varies throughout the initial, second, and third crop periods (Nugrahaeni et al. 2021). Moreover, seed size is crucial because it determines the number of stored food reserves. Different bulbs' diameters also affect seed growth rate, with larger bulbils growing more rapidly. Larger-weight seed is superior to tiny ones due to their petiole length viability. The heavier the bulbils, the greater the buds, fresh plant weight, plantlet height, shoot and root dry weight, tuber diameter, thickness, and harvest corm weight produced (Soedarjo and Sasmita 2021; Ibrahim et al. 2022). Furthermore, it is possible to propagate seeds by cutting bulbils, which typically have protuberances on the surface, known as tubercles, eventually growing into candidate shoots (Harijati and Ying 2021). The success of porang farming relies on seed availability in adequate quantity and with superior physiological quality (Riptanti et al. 2022).

Bulbils are collected when the petiole spontaneously detaches, showing complete dormancy. The quality is determined by their full dormancy state, without any sign of rotting, peeling, or fungal infections (Sari 2015; Hidayah et al. 2018). However, porang seeds are not available throughout the year in Indonesia. Farmers conduct forceful harvests before the plants are completely dormant to meet the demand, causing injuries and preventing the bulbils from achieving appropriate storage humidity (Sari et al. 2019). Incorrect handling and storage might also cause porang seed to be harmed. Newly fallen bulbils, specifically non–dominant types, can spread undetected infections due to the high moisture content of the seed. The presence of pathogens in the form of fungi hinders plant development, decreasing embryo germination, vigour, and seed composition. Moreover, infection reduces the quality, viability, germination, growth, and growth of seed, leading to diminished yield productivity (Alemu 2019; Turner et al. 2020; Soedarjo and Sasmita 2021).

The timing of fresh shoot emergence depends on the dormancy status of the planting material. When the plant material has completed its dormancy before planting, a new shoot will sprout almost immediately after being transplanted. However, in cases where the apical buds of the seed are injured, leaf emergence is delayed after planting. As stated in a previous study, bulbils require two to three weeks from planting to initiate sprouting (Ravi et al. 2011). The problem of nonviable seed from bulbils may result in losses when subsequently planted. Furthermore, conducting planting tests is time-consuming, and the high demand for porang seed requires quick fulfilment. To meet this demand, a fast and real-time method such as computer vision is needed to detect quality as a non-destructive, cost-effective, and dependable technology.

Image classification, which relies on gray–level cooccurrence matrix (GLCM) features including energy, contrast, homogeneity, dissimilarity, and correlation, combined with a backpropagation algorithm on an artificial neural network (ANN), has successfully detected and classified porang leaf disease with a regression coefficient as well as root mean square error (RMSE) of 0.9 and 0.5, respectively (Tsaqib and Rimantho 2022). Therefore, this study aimed to use computer vision to investigate colour and texture based on GLCM for image classification. This will facilitate the differentiation of non–infected and infected bulbils in real–time and thoroughly before planting.

MATERIALS AND METHODS

Plant materials and growth condition. Samples of porang were sorted manually into non-infected and fungi or fleas-infected seeds. From June–August, the bulbils were harvested in the third and fourth vegetative phases by farmers in the Karangmojo area, Kalasan, Yogyakarta, Indonesia. The samples used in the non-destructive method included

https://doi.org/10.17221/79/2023-RAE

90 seeds of both qualities. The differences between non-infected and infected bulbils are shown in Figure 1. The physical properties were measured by weight, side diameter, upper diameter, and spherical volume. The weight was assessed with an analytical balance (Fujitsu FS-AR), while the spherical volume was measured based on the average side and upper diameter using a caliper (Equation 1).

$$1.333 \times \pi \times \left(\frac{d_1 + d_2}{2} \right)^2 \quad (1)$$

where: d_1 – side diameter; d_2 – upper diameter

Porang seed, with an initil moisture content of 75.00 ± 0.50%, were germinated and cultivated in a mixture of soil, compost, and husk charcoal as planting medium (approximately 150 g; pH 7.0). Planting was carried out in an iron-framed growth chamber using sunlight with para net coverage (min. 70 and max. 880 of daily lux, 30.00 ± 3 °C of temperature, 80.00 ± 5% of relative humidity). Fresh and dry weight, root length, root volume, plant height, number of leafs, and plant canopy were measured as growth parameters after 60 d of cultivation. The plant canopy measurement was based on the longest leaf diameter (Equation 2).

$$\pi \times \left(\frac{d_1 + d_2}{4} \right)^2 \quad (2)$$

Image acquisition. Image acquisition was carried out by capturing a single image on each object three times with different sides using the Logitech C270 720P (Indonesia) webcam, with black paper as a background. The CMOS sensor of the webcam turns light into electrical signals, providing high-speed signal readout, low power consumption, small size, and programmability (Radha Krishna et al. 2021). The resolution accurately depicted porang seed and was considered ideal for this exploratory study. The image acquisition process took place inside an enclosure box designed to prevent external light interference. The shooting distance was fixed at 15 cm, centred on the bulbils, while illumination inside the enclosed box was achieved with an artificial ring light. The image was entered into an image processing program created through Python (version 3.10.1), with a resolution of 720P (1280 × 720 pixels) (Figure 2).

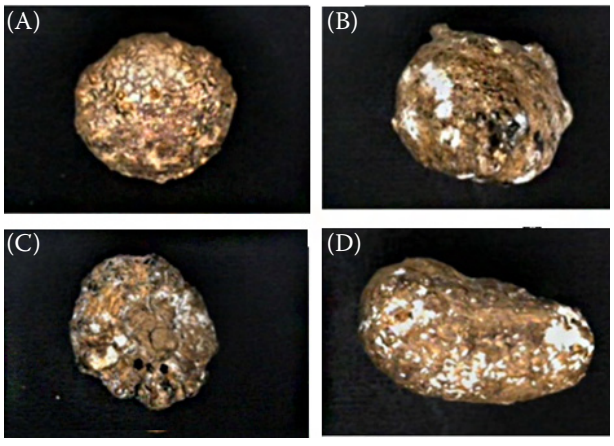

Figure 1. The study used (A) non–infected, (B) moldy, (C) dried, and (D) lice-infested bulbils

Three plates were calibrated before image acquisition, including white, dark, and dotted for surface reflectance correction, background correction, and geometric pixel positioning respectively. Subsequently, the Kernel value was applied as the convolutional matrix on image. Image for the bulbils was analysed by converting it into a binary image using thresholding. This process effectively separated the object by transforming the background to black through image segmentation. To separate objects from image, improve pixel accuracy, and reduce background noise, a 7 by 7-pixel structured element was used as an opening and closing operation to maintain object size. Image was then examined for colour (red, green, blue – RGB and hue, saturation, intensity – HSI), texture (contrast, correlation, homogeneity, energy, and entropy), and dimensions (width, height, and area) based on GLCM (Table 1). The GLCM was used to derive texture properties, including contrast (in pixel values), correlation (the degree of linearity between pixel values), entropy (pixel value randomness), energy (pixel value uniformity), and homogeneity (pixel value consistency). The object dimensions (width, height, and area) were calculated using the concept of a bounding rectangle that aided in object detection and identification within image (Syahputra et al. 2019). The image acquisition and extraction procedures before discriminant analysis and model performance are summarised in Figure 3.

Statistical and model performance analysis. Multivariate analysis of variance (MANOVA), independent sample *t*-test, and Pearson correlation analysis were used to investigate the different characteristics of non-infected and infected porang bulbils, as well as the relationship between their physical, vegetative growth, and imaging attributes. The data were analysed using SPSS software (version 25), while GraphPad Prism (version 9.0.0.) produced the

https://doi.org/10.17221/79/2023-RAE

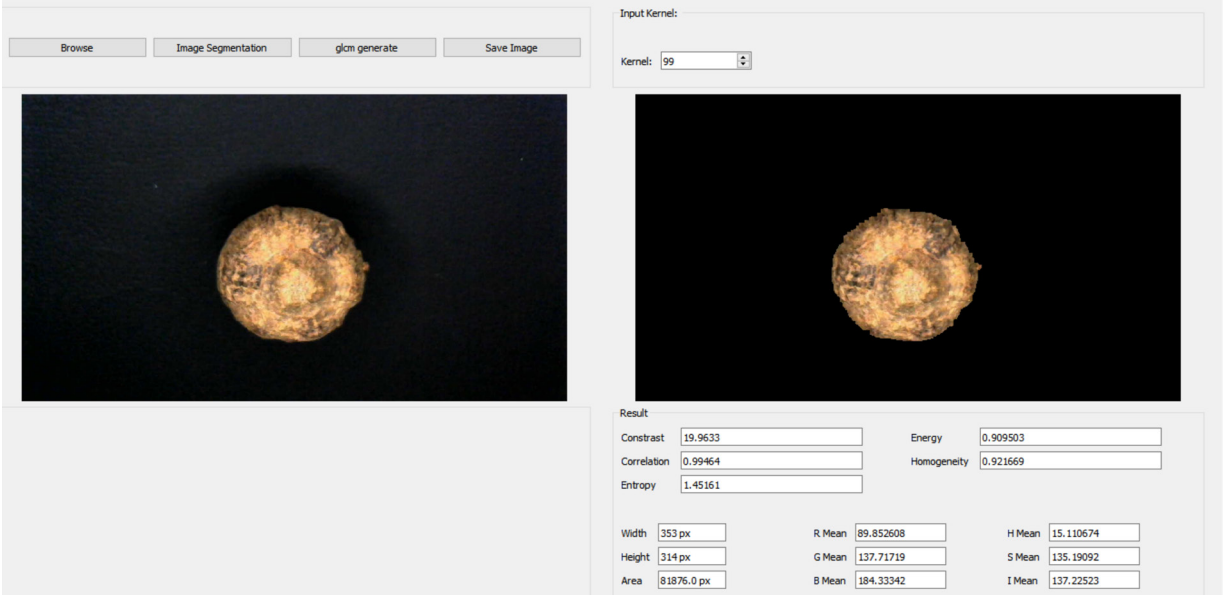

Figure 2. The graphical user interface of the image processing application

Table 1. Image feature formula

Image features	Formula
Colour conversion	
Hue	$z\begin{cases}\theta & if\ b \le g \\ 360-\theta & if\ b > g\end{cases}$
Saturation	$\theta = \cos^{-1}\left\langle \frac{\frac{1}{2}[(r-g)+(r-b)}{\sqrt[2]{(r-g)^2+(r-b)\times(g-b)}} \right\rangle$
Intensity	$\frac{(r+g+b)}{3}$
GLCM method texture	
Energy	$\sum_i \sum_j P_d^2(i,j)$
Entropy	$-\sum_i \sum_j P_d^2(i,j) \log P_d(i,j)$
Contrast	$\sum_i \sum_j P_d^2(i,j)(i-j)^2$
Homogeneity	$\sum_i \sum_j \frac{P_d^2(i,j)}{1+\lvert i-j \rvert}$
Correlation	$\sum_i \sum_j \frac{(i-\mu_x)(j-\mu_y)P_d(i,j)}{\sigma_x \sigma_y}$

z – hue value; θ – saturation value; g – green; b – blue; r – red; i – rows in the GLCM matrix; j – columns in the GLCM matrix; P_d – value at position (i, j) in normalised GLCM; μ_x, μ_y – the average intensity of pixels along the i- and j-axis, respectively; σ_x, σ_y – the standard deviation of pixel intensities along the i-axis and j-axis, respectively; GLCM – gray–level cooccurrence matrix

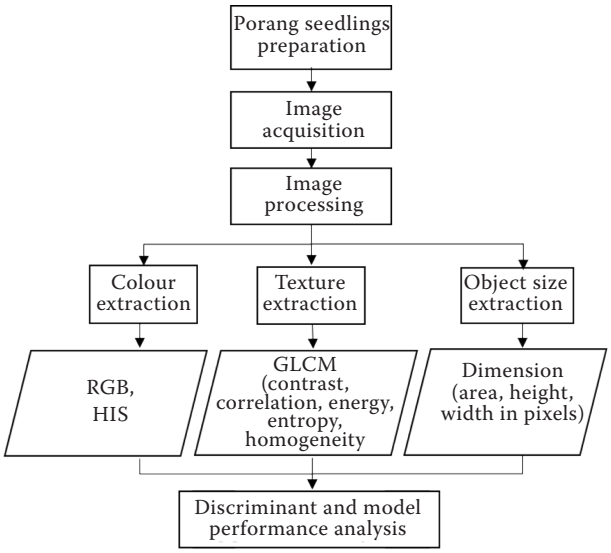

Figure 3. Process of an image acquisition and data extraction of colour, dimension, and gray–level cooccurrence matrix (GLCM)

RGB – red, green, blue; HIS –hue, intensity, saturation

heatmaps for Pearson's correlation. Twenty samples were tested for statistical analysis with a significance level of 5%. Discriminant analysis was used to classify and validate objects in these groups based on their image attributes, using 90 non-infected and infected samples. To reduce bias that may occur in the classification process, the leaf-one-out-cross-validation method was used. As the logical extreme of K–fold cross-validation, all training and validation data sets

https://doi.org/10.17221/79/2023-RAE

Table 2. Model performance analysis

Model performance	Formula
R^2	$\frac{\left[\sum\left(Y_{ref}-\overline{Y}_{ref}\right)\left(Y_{pred}-\overline{Y}_{pred}\right)\right]^2}{\left[\sum\left(Y_{ref}-\overline{Y}_{ref}\right)^2\sum\left(Y_{pred}-\overline{Y}_{pred}\right)\right]}$
MAE	$\frac{1}{n}\sum_{i=1}^{n}\lvert y_i-\hat{y}_i\rvert$
RMSE	$\sqrt{\frac{1}{n}\sum_{i=1}^{n}\left(y_i-\hat{y}_i\right)^2}$
Accuracy	$\frac{TN+TP}{TN+TP+FP+FN}\times 100\%$
Relilability	$\frac{TN}{TN+FP}+\frac{TP}{TP+FN}-1\times 100\%$
Specificity	$\frac{TN}{TN+FP}$
Sensitivity	$\frac{TP}{TP+FN}$

R^2 – the coefficient of determination; MAE – mean absolute error; Y – value; $\bar{Y}$– average of the value; $\hat{Y}$– predicted value; n – number of observations; reference; pred – prediction; TN – true negative; TP – true positive; FN – false negative; FP – false positive

were processed with the leave-one-out (LOO) method. The fold count was equal to the number of data points in the original data sets (Zahra et al. 2022). The performance assessment of discriminant analysis model was evaluated from the value of MAE, RMSE, accuracy, reliability, specificity, and sensitivity (Table 2).

RESULTS AND DISCUSSION

Physical, vegetative growth, and image quality properties of porang bulbils. There was a significant difference between the upper diameter and initial weight parameters of non–infected and infected seed based on the *t*-test results (Table 3). The initial weight of infected bulbils was significantly lower than non-infected ones and typically tended to have a small side diameter but a higher upper diameter. Infected bulbils were contaminated with fungi and other microbes, and the endosperm in tubers served as a food source for fungi, which affected their weight (Sari et al. 2019). In contrast, A'yun et al. (2019) found that the diameter and weight of seed during harvest strongly correlated with the time and phase of harvesting. Aside from influencing the dimensions based on image properties, these results produced considerable variances in width, height, and area. Significant dimensions in the form of width, height, and area in pixels show that the dimensional factors affect quality of the bulbils. Based on the acquired values, the diameters of infected bulbils were greater than non–infected ones, which was attributed to the irregular and non-uniform shape on multiple sides.

The colour parameters (R – reed, G – green, H – hue, S – saturation, and I – intensity) showed statistically significant variations between non-infected and infected bulbils. Significant colour analysis showed that image parameters R, G, H, S, and I influenced the quality of the bulbils. The R and G values of non-infected bulbils were greater than those of infected ones. In this study, the RGB colour model was converted to HSI values. Due to the device-specific properties of RGB colour spaces, normalisation of RGB colour spaces was required. In addition, hue, saturation, and intensity (HSI) space, which is closer to how humans perceive colour, is frequently used in food and agricultural inspection (Cubero et al. 2011). HSI space has been recommended as an efficient colour selection method for image segmentation in graphic applications. HSI model is used extensively in image processing and computer vision because it closely resembles human colour perception and is a popular colour–mixing method (Tsaqib and Rimantho 2022; Zahra et al. 2022). In this study, the colour reading of the HSI model showed that the non–infected bulbils had higher saturation and intensity values but a lower hue. The saturation and intensity values showed that overall colour was more distinct or dense and brighter than that of infected bulbils.

The texture is the regularity of patterns formed by digital image pixel configurations. Furthermore, GLCM method analyses texture and produces contrast, correlation, entropy, energy, and homogeneity values (Tsaqib and Rimantho 2022). Significant texture analysis results showed that texture characteristics influenced the quality of bulbils. Infected bulbils had more excellent contrast and entropy than non–infected ones, showing that infected bulbils have a more random texture due to their high entropy and contrast values. The variation of entropy

Research in Agricultural Engineering, 70, 2024 (2): 111–121

https://doi.org/10.17221/79/2023-RAE

Table 3. Physical, vegetative growth, and image properties of porang bulbils

Parameter	Non–infected				Infected				Significance	Partial Eta squared
	min	max	mean	SD	min	max	mean	SD		
Physical properties										
Initial weight (g)	4.91	6.87	5.78[b]	0.66	3.35	6.42	4.31[a]	4.31	*	0.489
Side diameter (mm)	22.85	28.18	24.77[a]	1.48	20.46	32.17	24.09[a]	3.10	ns	0.021
Upper diameter (mm)	15.67	19.63	17.86[b]	1.11	14.12	18.90	16.44[a]	1.16	*	0.291
Spherical volume (mm^3)	3 931.00	6 641.26	5 114.59[b]	840.28	3 087.30	7 963.53	4 444.77[a]	1222.86	*	0.097
Vegetative growth										
Root fresh weight (g)	0.44	1.82	0.97[a]	0.31	0.40	2.31	0.92[a]	0.49	ns	0.008
Shoot fresh weight (g)	16.59	38.67	26.65[b]	5.76	3.28	25.60	13.68[a]	5.21	*	0.595
Root dry weight (g)	0.10	0.21	0.14[a]	0.03	0.07	0.40	0.15[a]	0.08	ns	0.004
Shoot dry weight (g)	0.50	1.35	0.83[b]	0.22	0.13	1.02	0.57[a]	0.20	*	0.289
Root length (cm)	18.00	34.50	24.97[b]	3.81	10.00	26.50	19.67[a]	4.14	*	0.275
Root volume (cm^3)	0.50	2.00	1.03[a]	0.26	0.50	2.00	1.03[a]	0.38	ns	0.001
Plant height (cm)	40.70	64.00	54.03[b]	5.68	19.50	50.40	38.23[a]	8.88	*	0.542
Plant canopy (cm^2)	1 301.53	3 391.54	2 081.31[b]	666.35	359.83	1 772.78	1 127.62[a]	401.53	*	0.442
Image Properties										
Red	69.35	113.90	86.80[a]	10.63	73.89	104.69	85.65[a]	8.88	ns	0.004
Green	104.59	149.87	124.86[b]	11.42	104.57	134.51	117.96[a]	8.10	*	0.113
Blue	142.07	185.71	164.05[b]	12.34	131.01	164.62	149.06[a]	9.27	*	0.332
Hue	14.51	15.51	14.86[b]	0.22	15.45	17.90	16.33[a]	0.64	*	0.715
Saturation	95.06	125.66	108.55[b]	7.75	74.95	108.17	91.15[a]	10.00	*	0.499
Intensity	105.79	149.64	125.53[b]	11.12	104.21	133.51	117.45[a]	7.93	*	0.155
Width (px)	304.33	375.00	331.17[a]	20.94	294.67	471.00	349.55[a]	44.05	ns	0.070
Height (px)	276.33	339.67	304.55[a]	16.12	269.33	360.67	302.18[a]	25.10	ns	0.003
Area (px)	64 943.67	85 649.83	73 324.41[a]	6 602.70	60 374.50	109 002.33	76 797.68[a]	14 149.74	ns	0.025
Contrast	15.18	23.90	18.08[b]	2.35	16.91	34.67	25.86[a]	5.12	*	0.501
Correlation	0.99	0.99	0.99[a]	0.00	0.99	0.99	0.99[a]	0.00	ns	0.050
Entropy	1.27	1.66	1.41[b]	0.11	1.41	1.99	1.73[a]	0.16	*	0.595
Energy	0.91	0.93	0.92[a]	0.01	0.88	0.93	0.92[a]	0.02	ns	0.016
Homogeneity	0.92	0.94	0.93[a]	0.01	0.89	0.94	0.93[a]	0.01	ns	0.036

[a, b] numbers with different letters indicates a statistically significant mean difference between non-infected and infected groups by the independent sample t-test at $P < 0.05$; *, ns – the row with different letters shows a statistically significant or not-significant between non-infected and infected groups (MANOVA, $P < 0.05$)

https://doi.org/10.17221/79/2023-RAE

can explain sample behaviour over time, with higher entropy values implying greater image randomness (Anjna et al. 2020; Omidi-Arjenaki et al. 2020). Non–infected bulbils had more significant correlation, energy, and homogeneity values than infected ones, showing a more uniform texture due to their high homogeneity and energy values; the greater the homogeneity, the bigger the energy value. Homogeneity is used to evaluate the uniformity and pixel clarity of an image, which is the opposite of contrast (Anjna et al. 2020).

Statistically significant differences ($P < 0.05$) were found in the majority of vegetative growth parameters between non–infected and infected porang bulbils, including shoot fresh weight, dry weight, root length, plant height, and plant canopy (Table 3). Fungal infection negatively impacts plant growth and development, including germination rates, hypocotyl length, root length, fresh weight, and dry weight after planting. In addition, the transmission of severe seed-borne diseases related to porang cultivation, particularly affecting the bulbil, can occur through infected seed mainly contaminated by tuber fungi, such as *Phytophthora colocasiae, Sclerotium rolfsii, Fusarium solani, Fusarium oxysporum,* and *Botrytis cinerea* (Sakaroni et al. 2019; Tiwari et al. 2020; Soedarjo and Djufry 2021). Seed-borne illness refers to the transmission of inoculum through seed, which can impede the growth of sprouts and result in losses of up to 25%. Furthermore, the infection rate during storage can reach up to 60%. Seed-borne diseases significantly impact the planting process, leading to plant damage, decreased harvest output, and a potential source of further infection in both seed and nearby plants. Previous studies also observed that certain pathogenic fungi, including *Fusarium* species, generated mycotoxins within food-related products (Tiwari et al. 2020; Meriles et al. 2004).

Classification of seed quality based on image properties. The classification of bulbils quality based on image parameters was performed using discriminant analysis, with image parameter data integrated into the discriminant function. The discriminant analysis assumes that data meet the requirements of the linearity, normality, multilinearity, and equality of variance tests. This ensures that analysis can optimally separate groups with a specific degree of distinction (Ahmad et al. 2018; Zahra et al. 2022). Based on the results, function 1 had an eigenvalue of 3 985 and a canonical correlation of 0.89, which explained 100% of the variance (Table 4). This high degree of discrimination was attributed to the relatively high closeness value. Canonical correlation can quantify the degree of proximity between discriminant values and groups (Ahmad et al. 2018; Zahra et al. 2022). In addition, function 1 had a Wilks Lambda value of 0.201, equivalent to a Chi-square (χ^2) value of 423.282, and a significance of 0.00 for every image parameter. This score implied that each quality differed significantly between the groups.

Based on the matrix structure, function 1 had the strongest link with the order correlation, saturation, and red value, showing that the correlation was most closely related to the discriminant function. Matrix structure describes the relationship between the independent variables and the discriminant function (Ahmad et al. 2018; Zahra et al. 2022). According to the canonical discriminant function coefficients, the correlation has the highest value, showing a close relationship between the linkage and discriminant function. These coefficients determine if a case belongs to a particular group and show that many predictor factors form discriminant function. By calculating the discriminant score, the discriminant function was used to validate predictions in the initial validation stage (Ahmad et al. 2018; Zahra et al. 2022). Intensity provides a considerable capacity for discrimination based on the standardised canonical discriminant function coefficients. In the blue parameters (B), height, area, energy, and homogeneity, a subset showed that these variables were not used in the investigation. B was not used since the *t*-test did not show a significant difference, while height, area, energy, and homogeneity were not used because the significance *F* was greater than 0.05. This implied that the five variables did not satisfy the constraints of the discriminant model (Table 5).

Using Fisher's linear discriminant method, a discriminant model was created to classify bulbil quality (Table 6). The derived equations were then validated in the program by entering the extracted

Table 4. Wilks' lambda value and eigenvalue

Parameter	Values
Test of function(s)	1
Wilks' lambda	0.201
Chi-square	423.282
Significance	0.000
Eigen value	3.985
Percent of variance (%)	100.0
Canonical correlation	0.894

https://doi.org/10.17221/79/2023-RAE

Table 5. Structural matrix, canonical discriminant coefficient function, group mean test in image processing of bulbils

Discrimination coefficient of image properties	Structure matrix	Stand. canonical discriminant function coefficients	Canonical discriminant function coefficients	Tests ofequality of group means	
	1	1	1	Wilks' lambda	Significance
Constant			632.322		
Blue[a]	–0.025			0.997	0.401
Green	0.100	–9.567	–0.762	0.962	0.001
Red	0.252	–4.818	–0.350	0.798	0.000
Hue	–0.570	–0.537	–0.831	0.436	0.000
Saturation	0.463	1.493	0.140	0.539	0.000
Intensity	0.130	13.100	1.073	0.937	0.000
Width	–0.262	–0.301	–0.008	0.786	0.000
Height[a]	–0.070			0.944	0.000
Area[a]	–0.186			0.838	0.000
Contrast	–0.391	1.094	0.169	0.622	0.000
Correlation	0.468	1.203	657.470	0.534	0.000
Entropy	–0.507	–0.509	–2.898	0.494	0.000
Energy[a]	0.187			0.840	0.000
Homogeneity[a]	0.211			0.821	0.000

[a] variable not used in discriminant analysis

Table 6. Discriminant classification model of porang bulbils

Parameter	Bulbil quality	
	non-infected	infected
Red	–364.959	–363.567
Green	–545.616	–542.586
Hue	30.874	34.177
Saturation	139.280	138.725
Intensity	754.896	750.629
Width	–23.929	–23.896
Contrast	290.614	289.942
Correlation	1 515 869.186	1 513 254.065
Entropy	904.798	916.326
(Constant)	–743 518.940	–741 003.848
Group centroids	1.989	–1.989

image parameter values R, G, H, S, I, width, contrast, correlation, and entropy. The non-infected and infected scores represented quality groups derived from the image-processing calculation of image parameter values. Based on the results, each quality had a unique discriminant score that operated as a criterion or value separator.

Table 7 showed that the prediction of most group members was consistent with the amount of initial data, both original and cross-validated. The results of the prediction show the percentage of accuracy after grouping. In the original column, non–infected bulbils were accurately classified in 133 samples (98.5%), while 2 samples were incorrectly predicted as infected (1.5%). 130 samples were adequately classified as infected (96.3%), while 5 infected samples (1.8%) were incorrectly predicted as non-infected.

Leave-one-out cross-validation (LOOCV) is used in the classification process to limit the possibility of bias (Zahra et al. 2022). In the cross-validated column of non–infected samples, 133 (98.5%) were correctly classified, while 2 (1.5%) were incorrectly predicted. A total of 129 infected samples (95.6%) were

Table 7. Results of discriminant test classification based on image parameters

	Initial quality	Prediction (amount/%)		Total (amount/%)
		non-infected	infected	
Original[a]	non-infected	133 (98.5)	2 (1.5)	135 (100)
	infected	5 (3.7)	130 (96.3)	135 (100)
Cross–validation[b]	non-infected	133 (98.5)	2 (1.5)	135 (100)
	infected	6 (4.4)	129 (95.6)	135 (100)

[a] 97.4% of original grouped cases were correctly classified; [b] 97.0% of cross-validated grouped cases were correctly classified

https://doi.org/10.17221/79/2023-RAE

correctly classified, while 6 (4.4%) were incorrectly predicted. The obtained accuracy values were comparable and classified as high classification accuracy. The high accuracy implies that the computer vision system has successfully classified different qualities of bulbils.

The obtained results were then validated using sensitivity, specificity, accuracy, false positive rate (FPR), false negative rate (FNR), reliability, RMSE, and MAE criteria (Table 8). The relative proximity of the sensitivity and specificity values to 1 shows that the calibration and validation models are suitable for classifying bulbils into two distinct qualities. The optimal model has high sensitivity, specificity, and validity (Rashvand and Akbarnia 2019; Anjna et al. 2020; Saputro et al. 2022). Based on the FPR and FNR values of the calibration and validation model, a value close to 0 was obtained, showing that the model had excellent performance. In addition, the values for accuracy and reliability were close to 1, implying that the resulting model was acceptable. A perfect model has precision and dependability values close to 1 as well as FNR and FPR values near 0 (Rashvand and Akbarnia 2019; Anjna et al. 2020; Prastiwi et al. 2023). Furthermore, the RMSE and MAE values were close to 0, showing that the prediction outputs of the model were accurate. As stated by previous studies MAE and RMSE values close to zero show good performance or accuracy of the prediction model (Rashvand and Akbarnia 2019; Nurrahmah et al. 2023; Rahmawati et al. 2023). According to the results of the discriminant model with image parameters, it was considered applicable for classifying bulbils of different quality.

The correlation between physical and vegetative growth properties and image quality of porang bulbils. Pearson's correlation heatmaps depicts the relationship between physical, vegetative growth and image properties in the non-infected and infected porang bulbils (Figure 4). The physical and vegetative growth quality had differential effects on the properties of bulbil image. A significant positive correlation was observed between image characteristics of width, height, and area with quality of initial weight, side diameter, and spherical volume in both non-infected and infected seed.

Table 8. Model performance based on image parameters

Model performance	Calibration	Validation
Sensitivity	0.96	0.96
Specificity	0.99	0.99
FPR	0.01	0.01
FNR	0.04	0.04
Accuracy	0.97	0.97
Reliability	0.95	0.94
RMSE	0.16	0.17
MAE	0.03	0.03

FPR – false positive rate; FNR – false negative rate; RMSE – root mean square error; MAE – mean absolute error

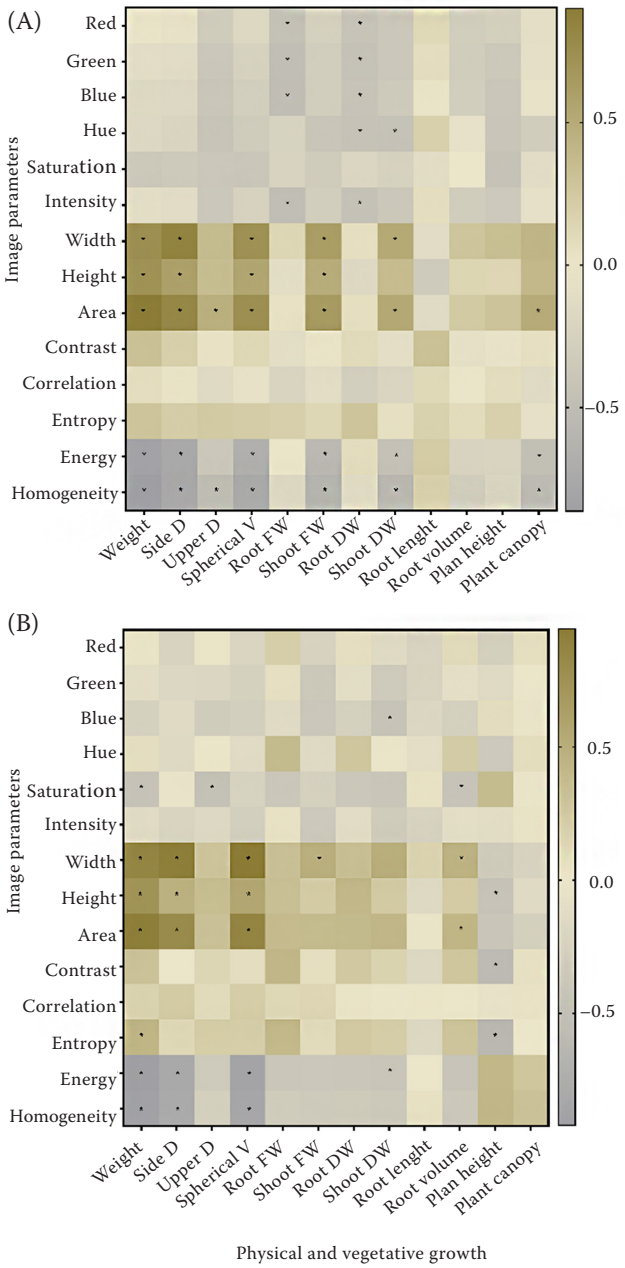

Figure 4. Heatmap showing Pearson's correlation between the physical, vegetative growth, and image properties of (A) non-infected and (B) infected porang bulbil

* indicates a significance at $P \leq 0.05$

https://doi.org/10.17221/79/2023-RAE

On the other hand, significant inverse associations were observed between energy and homogeneity, with initial bulbil weight, side diameter, and spherical volume. Image attributes including R, G, B, H, I, width, height, area, energy, and homogeneity had a moderate correlation with the fresh and dry weight of roots and shoots, as well as the canopy of the plant, during the vegetative growth stage of non–infected seed. In contrast, there was a moderate correlation between some image attributes (including B, S, width, height, area, contrast, entropy, and energy) with shoot fresh and dry weight, root volume, and plant height of infected bulbils. The greater the response in a positive correlation, the higher the strength of the variable predictor, while in a negative correlation, the response decreases as the variable predictor increases (Zahra et al. 2022). Generally, a Pearson correlation coefficient value greater than 0.50 shows the presence of multicollinearity, referring to the occurrence of high intercorrelations, most commonly in non-infected porang bulbils.

CONCLUSION

In conclusion, the physical features and vegetative growth of the seed showed that the weight, spherical volume, shoot fresh and dry weight, root length, plant height, and canopy differed between infected and non-infected bulbils. Infected porang bulbils varied in colour and image textural properties compared to non–infected ones. Furthermore, discriminant analysis effectively classified the quality of porang bulbils with the following attributes: accuracy (97.4%), model sensitivity (0.96), specificity (0.99), FPR (0.01), FNR (0.04), reliability (0.95), RMSE (0.16), and MAE (0.03). The discriminant method was effective for assessing the quality of various bulbils using image parameters, as shown by the model's high accuracy and good performance. The Pearson correlation heatmap showed multicollinearity in non-infected and infected bulbils with significant physical, vegetative growth, and image properties relationships up to 0.943. These results can be used in developing a porang quality evaluation system, which is critical for seed industry quality procedures.

Acknowledgement: We express our gratitude for the laboratory facilities provided by the Biological Physics Laboratory, Department of Agricultural and Biosystems Engineering, Faculty of Agricultural Technology at Universitas Gadjah Mada, Indonesia. The authors also would like to extend our appreciation for the collaboration provided by the porang Farmer in Kalasan, Yogyakarta, Indonesia, regarding the bulbil of porang.

REFERENCES

Ahmad U., Bermani D.P., Mardison. (2018): Color distribution analysis for ripeness prediction of Golden Apollo Melon. Telkomnika (Telecommunication Computing Electronics and Control), 16: 1659–1666.

Alemu G. (2019): Review on the effect of seed source and size on grain yield of bread wheat (Tritium Aestivum L.). Journal of Ecology & Natural Resources, 3: 1–8.

Anggela A., Setyaningsih W., Wichienchot S., Harmayani E. (2021): Oligo–glucomannan production from porang (Amorphophallus oncophyllus) glucomannan by enzymatic hydrolysis using β–mannanase. Indonesian Food and Nutrition Progress, 17: 23–27.

Anjna S.M., Singh P.K. (2020): Hybrid system for detection and classification of plant disease using qualitative texture features analysis. Procedia Computer Science, 167: 1056–1065.

A'yun Q., Harijati N., Mastuti R. (2019): The selection technique of bulbil porang (Amorphophallus muelleri Blume) based on growth response. Journal of Environmental Engineering & Sustainable Technology, 6: 30–35.

Cubero S., Aleixos N., Moltó E., Gómez–Sanchis J., Blasco J. (2011): Advances in machine vision applications for automatic inspection and quality evaluation of fruits and vegetables. Food and Bioprocess Technology, 4: 487–504.

Dermoredjo S.K., Azis M., Saputra Y.H., Susilowati G., Sayaka B. (2021): Sustaining porang (Amorphophallus muelleri Blume) production for improving farmers' income. In: IOP Conference Series Earth and Environmental Science, 648: 1–10.

Harijati N., Ying, D. (2021). The effect of cutting the bulbil–porang (Amorphophallus muelleri) on its germination ability. In: IOP Conference Series Earth and Environmental Science, 743: 1–8.

Hidayah N., Suhartanto M.R., Santosa E. (2018): Growth and production of iles–iles (Amorphophallus muelleri blume) seeds from different cultivation techniques. Buletin Agrohorti, 6: 405–411.

Ibrahim M.S.D., Sulistiyorini I., Tresniawati C. (2022): Effect of 6–benzyl amino purine on the multiplication ability of shoots of various sizes of porang (Amorphophallus muelleri Blume) bulbils. In: IOP Conference Series Earth and Environmental Science, 974: 1–9.

Meriles J.M., Lamarque A.L., Labuckas D.O., Maestri D.M. (2004): Effect of fungal damage by Fusarium spp and Diaporthe/Phomopsis complex on protein quantity and quality of soybean seed. Journal of the Science of Food and Agriculture, 84: 1594–1598.

https://doi.org/10.17221/79/2023-RAE

Nugrahaeni N., Hapsari R.T., Trustinah I.F.C., Sutrisno A.A., Yusnawan E., Mutmaidah S., Baliadi Y., Utomo J. S. (2021): Morphological characteristics of Madiun 1, the First Porang (Amorphophallus muelleri Blume) released cultivar in Indonesia. In: IOP Conference Series Earth and Environmental Science, 911: 1–7.

Nurlela N., Ariesta N., Santosa E., Muhandri T. (2022): Physicochemical properties of glucomannan isolated from fresh tubers of Amorphophallus muelleri Blume by a multilevel extraction method. Food Research, 6: 345–353.

Nurrahmah N.A., Zahra A.M., Rahayoe S., Masithoh R.E., Rahmawati L. (2023): Mathematical model of vegetative growth of porang (Amorphophallus muelleri) with different seed quality. In: Proceedings of the International Conference on Sustainable Environment, Agriculture and Tourism, Bangka, Indonesia, Jul 21–23: 245–253.

Omidi–Arjenaki O., Ghanbarian D., Mollazade K., Naderi–Boldaji M. (2020): Biospeckle imaging for evaluating mechanical properties of potato tubers during storage, part II: biospeckle in compression and creep tests. Journal of Food Measurement and Characterization, 14: 2209–2219.

Prastiwi F.D., Zahra A.M., Rahayoe S., Masithoh R.E., Pahlawan M.F.R., Nurrahmah N.A., Indrayanti E. (2023): The rapid detection of the infected seedlings of Amorphophallus muelleri using Visible Near–Infrared spectroscopy. Food Research, 7: 289–296.

RadhaKrishna M.V.V., Govindh M.V., Veni P.K. (2021). A review on image processing sensor. In: IOP Conference Series Journal of Physics, 1714: 1–8.

Rahmawati L., Zahra A.M., Listanti R., Masithoh R.E., Hariadi H., Syafutri, M.I., Lidiasari E., Amdani R.Z, Puspitahati, Agustini S., Nuraini L, Volkandari S.D., Karimy M.F., Suratno, Windarsih A., Pahlawan, M.F.R. (2023): Necessity of Log (1/R) and Kubelka–Munk transformation in chemometrics analysis to predict white rice flour adulteration in brown rice flour using visible–near–infrared spectroscopy. Food Science and Technology, 43: 1–8.

Rashvand M., Akbarnia A. (2019): The feasibility of using image processing and artificial neural network for detecting the adulteration of sesame oil. AIMS Agriculture and Food, 4: 237–243.

Ravi V., Ravindran C.S., Suja G., George J., Nedunchezhiyan M., Byju G., Naskar S.K. (2011): Crop physiology of elephant foot yam [Amorphophallus paeoniifolius (Dennst. Nicolson)]. Advances in Horticultural Science, 25: 51–63.

Riptanti E.W., Irianto H., Mujiyo. (2022): Strategy to improve the sustainability of "porang" (Amorphophallus muelleri Blume) farming in support of the triple export movement policy in Indonesia. Open Agriculture, 7: 566–580.

Sakaroni R., Suharjono S., Azrianingsih R. (2019): Identification of potential pathogen fungi which cause rotten on Porang (Amorphophallus muelleri Blume) tubers. In: Proceeding of the International Conference on Biology and Applied Science, Malang, Indonesia, Mar 13–14: 1–8.

Sarifudin A., Ratnawati L., Indrianti N., Ekafitri R., Sholichah E., Afifah N., Desnilasari D., Nugroho P., Yuniar A.D. (2022): Evaluation of some analytical methods for determination of calcium oxalate in Amorphophallus muelleri flour. Food Science and Technology, 42: 1–7.

Sari R.S. (2015): Porang plants: prospects for cultivation as one of the agroforestry systems. Info Teknis Eboni, 12: 97–110.

Sari M., Santosa E., Pieter L.A., Kurniawati A. (2019): Seed quality and seedling growth of iles–iles (Amorphophallus muelleri Blume) from different growing media. Indonesian Journal of Agricultural Sciences, 24: 144–150.

Soedarjo M., Djufry F. (2021): Identified diseases would threaten on the expansion of Amorphophallus muellery Blume cultivation in Indonesia. In: IOP Conference Series Earth and Environmental Science, 648: 1–10.

Soedarjo M., Sasmita P. (2021): Influence of growth media and bulbil sizes on plant growth and corm yield of porang (Amorphophallus muelleri Blume). In: IOP Conference Series Earth and Environmental Science, 911: 1–8.

Syahputra H., Indra Z., Febrian D., Adriani D.P. (2019): Leaf feature extraction using glcm, moment invariant and shape morphology for Indonesian medicinal plants recognition. In: IOP Conference Series Journal of Physics, 1317: 1–10.

Tiwari R.K., Kumar R., Sharma S., Sagar V., Aggarwal R., Naga K.C., Lal M.K., Chourasia K.N., Kumar D. and Kumar M. (2020): Potato dry rot disease: current status, pathogenomics and management. Biotech, 10: 1–18.

Tsaqib M.F.A., Rimantho D. (2022): Applying image classification for detect leaf disease: case study for porang plant. In: Proceeding of the 9th International Conference on ICT for Smart Society: Recover Together, Recover Stronger and Smarter Smartization, Governance and Collaboration, Bandung, Indonesia, Aug 10–11: 1–5.

Turner R.E., Ebelhar M.W., Wilkerson T., Bellaloui N., Golden B.R., Irby J.T., Martin S. (2020): Effects of purple seed stain on seed quality and composition in soybean. Plants, 9: 1–10.

Yanuriati A., Marseno D.W., Rochmadi, Harmayani E. (2017): Characteristics of glucomannan isolated from fresh tuber of Porang (Amorphophallus muelleri Blume). Carbohydrate Polymers, 156: 56–63.

Zahra A.M., Chosa, T., Tojo, S. (2022): Fruit quality evaluation in the maturation process of blueberries using image processing. Indonesian Food and Nutrition Progress, 18: 41.

Received: June 30, 2023
Accepted: February 6, 2024
Published online: June 27, 2024